energies

MDPI

Article

Exploring the Bioenergy Potential of Microfluidics: The Case of a T-Micromixer with Helical Elements for Sustainable Energy Solutions

Abdelkader Mahammedi [1], Naas Toufik Tayeb [2], Kouider Rahmani [3], Awf Al-Kassir [4] and Eduardo Manuel Cuerda-Correa [5,*]

[1] Department of Technology, ZianeAchour University of Djelfa, Djelfa 17000, Algeria; a.mahammedi@uni.v-djelfa
[2] Gas Turbine Joint Research Team, University of Djelfa, Djelfa 17000, Algeria; t.naas@univ-djelfa.dz
[3] Research Laboratory Modeling Simulation and Optimization of Real Complex Systems, Djelfa 17000, Algeria; k.rahmani@univ-djelfa.dz
[4] Departamento de Ingeniería Mecánica, Energética y de los Materiales, Escuela de Ingenierías Industriales, Universidad de Extremadura, Avenida de Elvas s/n, 06006 Badajoz, Spain; aawf@unex.es
[5] Departamento de Química Orgánica e Inorgánica, Facultad de Ciencias, Universidad de Extremadura, Avenida de Elvas s/n, 06006 Badajoz, Spain
* Correspondence: emcc@unex.es; Tel.: +34-924489121

Abstract: This study explores the potential application of microfluidics in the field of bioenergy, with a particular focus on the energy potential of biogas derived from vine shoots, a locally abundant waste material. The enhanced mixing capability of a micromixer has been analyzed to make it suitable for microfluidic energy applications. Mixing index, pressure drop, and kinematic measurements within the T-micromixer with helical elements and their related mixing performances have been studied and validated using CFD for different values of Reynolds number (0.1–60) for laminar Newtonian miscible fluid. Geometrical characteristics were further examined to improve the mixing performance. Various values of twisted angles were evaluated and compared to choose the optimal angle. A new parameter, Q, was introduced to represent the ratio of vorticity square over the sum of vorticity square and deformation square intensities. Furthermore, the results of the numerical simulation were compared with the given data in the literature, showing a significant agreement, in addition to the fact that a high-quality mixture can be created with a geometry angle of 90°, and a mixing index above 0.99 can be obtained at low Reynolds numbers. The numerical investigation of the flow regimes of miscible fluid in the T-microkenics with the proposed angle can be utilized to develop the mixing performance of the micromixers in a wide variety of processes.

Keywords: biogas; vine shoots waste; computational fluid dynamics; pressure drop; mixing index; vorticity

check for updates

Citation: Mahammedi, A.; Tayeb, N.T.; Rahmani, K.; Al-Kassir, A.; Cuerda-Correa, E.M. Exploring the Bioenergy Potential of Microfluidics: The Case of a T-Micromixer with Helical Elements for Sustainable Energy Solutions. *Energies* **2023**, *16*, 7123. https://doi.org/10.3390/en16207123

Academic Editors: Antonio Barletta and Michele Celli

Received: 18 September 2023
Revised: 10 October 2023
Accepted: 13 October 2023
Published: 17 October 2023

Copyright: © 2023 by the authors. Licensee MDPI, Basel, Switzerland. This article is an open access article distributed under the terms and conditions of the Creative Commons Attribution (CC BY) license (https://creativecommons.org/licenses/by/4.0/).

1. Introduction

With the aim of decreasing reliance on fossil fuels and tackling escalating environmental issues like greenhouse gas emissions, scientists in the field of internal combustion engines have recently redirected their attention from traditional fossil fuels such as gasoline and diesel towards renewable alternatives like biogas and syngas [1]. Energy production from the thermal conversion of biomass constitutes a cost-effective, renewable, and widely available process. In fact, bioenergy accounts for up to 70% of total renewable energy production [2].

Particularly in biomass gasification, an incomplete combustion of biomass is performed, and a mixture of combustible gases, including methane, hydrogen, and carbon monoxide, is generated. Gasification can be regarded as an environmentally friendly and

economically feasible process where the emission of greenhouse gases is nearly negligible [3]. Gasification is usually performed by heating biomass in the presence of oxygen, air, or steam at temperatures around or above 800 °C. The so-generated biogas is a useful, high-value, and versatile product. Hence, an adequate study and planning of all the steps involved in biogas generation, treatment, transport, and storage is of the utmost importance.

Nevertheless, the influence of fluid flow has been very frequently overlooked. Recently, however, efforts have been made to couple Computational Fluid Dynamics with biokinetic models of reactors. By integrating fluid flow analysis, a more comprehensive understanding of the processes involved can be achieved [4]. CFD is a simulation technique used to analyze and predict the behavior of fluids and gases in various environments. CFD simulations are used to optimize the design of renewable energy systems, such as wind turbines [5] and solar panels [6], too. CFD simulations can also model water flows in rivers, dams, and reservoirs. This helps optimize hydropower systems and informs water resource management decisions [7]. CFD also plays a role in optimizing combustion processes in conventional power generation [8]. By improving combustion efficiency and reducing emissions, CFD contributes to more sustainable energy production from fossil fuels during the transition to cleaner alternatives [9]. CFD is also used to optimize the design and layout of energy infrastructure, such as cooling systems for power plants [10] and energy-efficient buildings [11]. Efficient infrastructure reduces energy waste and promotes sustainable energy use. CFD simulations can assess the environmental impact of energy projects, including the dispersion of pollutants from power plants or industrial facilities [12], and help ensure that energy systems are designed, operated, and optimized in ways that align with the overall goals of sustainable development and a transition to cleaner and more accessible energy sources. By accurately modeling fluid flows and energy transfer, CFD helps engineers design more efficient and effective renewable energy technologies, contributing to increased energy efficiency and the use of sustainable energy sources.

With the ongoing advancements in computer technology, the utilization of CFD and numerical methods for heat transfer analysis is increasingly gaining traction within the realm of bioenergy research. This enables a more widespread exploration of intricate flow, heat, and mass transfer attributes [13]. Thus, the integration of CFD with bioenergy and biofuels research has become increasingly important in the last few years [14]. Furthermore, CFD aids in analyzing fluid flow patterns within bioreactors, improving biogas production, and optimizing the design of biofuel production facilities [15]. Thus, the application of CFD in the fields of bioenergy and biofuels plays a crucial role in advancing sustainable energy solutions, reducing environmental impacts, and fostering a cleaner and more energy-efficient future. In this connection, microfluidics can be an adequate tool to analyze the process on the microscale as an exploratory stage before scaling up.

Microfluidics is a rapidly evolving field that focuses on the manipulation of small volumes of fluids on the microscale. One area of interest in microfluidics is the development of micromixers, devices that efficiently mix fluids at the microscale. The objective of a micromixer is to achieve rapid and efficient mixing of fluid streams to promote reaction kinetics or ensure homogeneous conditions for analysis. The use of the microfluidics approach exhibits important advantages, such as (i) reduced requirements in terms of reactants and sample amounts; (ii) shorter reaction times; (iii) lower production costs; and (iv) better heat transfer rates [16]. Microfluidic devices, including micromixers, are inherently compact and amenable to integration with other microfluidic components. Micromixers can be easily fabricated using microfabrication techniques and can be readily scaled up for higher-throughput applications. Thus, the application of microfluidics in the field of renewable energy has gained importance in the last few years [17,18]. However, due to the inherent laminar flow characteristics at the microscale, achieving efficient mixing can be challenging. In microfluidic systems, the laminar flow regime is predominantly used, and the mixing mechanism is molecular diffusion, which is very slow [19]. Therefore,

molecular diffusion increases the duration of the mixing process and requires long channels to achieve the desired mixing.

In this connection, geometry plays an essential role, beyond any doubt [20]. Different types of geometry can be used to achieve the chaotic mechanism [21–26]. In addition, the concept of chaotic mixing was discussed previously [27].

The mixing index is calculated using numerical techniques within the CFD framework [28]. By simulating the fluid flow and analyzing the scalar field distribution, the necessary quantities for computing the mixing index are obtained. The mixing index values can then be compared, and parametric studies can be conducted to optimize mixing conditions or assess the performance of mixing devices.

Most passive micromixers are designed with a Y or T shape for the initial contact of the fluids to be mixed [29,30]. The distinctive Y and T shape elements are frequently used in more complex microsystems [31], and they have been numerically and experimentally tested. The T-shaped micromixers are the most frequent among all possible types of microreactors and micromixers [32]. Wong et al. [33] gave an overall evaluation of the flow stream and mixing parameters in T-shaped micromixers. In this way, various changes in the device have been presented to increase the advection in mixing using 2D or 3D serpentine design, including barriers as obstacles or grooves and ridges within the channel [23,34,35].

Various specific configurations can be employed to significantly improve the heat transfer efficiency of Newtonian fluids [36]. The Newtonian agitation in a T-micromixer with multiple inlets has been experimentally illustrated. It has been revealed that the utilization of asymmetrical T-mixer pilots augments the quality of the mixture. Hoffmann et al. [37] experimentally investigated the velocity and concentration fields in T-shaped micromixers via μ-PIV and μ-LIF.

Numerical simulations have proven to be extremely useful tools in the analysis of micromixing, making it easier to understand such a complex process and enhancing the design of optimized microfluidic devices [38,39]. Cortes et al. [40] numerically studied the performance of the mixture in a three-dimensional passive T-mixer, which gives a rapid formation of vortical flow and high mixing with inferior pressure drop compared to a planar mixer. Gobby et al. [41] examined the parameters of the mixture in a micromixer for a gas flow of methanol and oxygen. The device studied is based on a T-shape [42]. The use of helical structures induces chaotic advection and enhances mixing by disrupting the laminar flow. The helical elements introduce vortices and stretch the fluid streams, leading to enhanced mixing performance. Kim et al. [16] presented a new passive mixer with helical elements called barrier-embedded Kenics (BEKM); they concluded that the BEKMs required mixing length outperforms two other T-shape micromixers. Bertsch et al. [43] tested experimentally and numerically a Y-micromixer composed of a series of short helix elements, commercialized by Kenics™. They evaluated the mixing efficiency with good mixing efficiency and less pressure drop. The velocity and mixing characteristics of Y and T micromixers can affect heat transfer rates, and efficient mixing can help achieve better temperature control and energy utilization in microscale devices. In general, Y-mixers are preferred when rapid mixing is required. However, the mixing in the T micromixer relies on diffusion and chaotic advection.

Vorticity is a fundamental concept in fluid dynamics that quantifies the local rotation of fluid elements within a flow. It is a vector field that describes the tendency of a fluid to rotate around an axis. The analysis of vorticity provides valuable insights into the structure, dynamics, and behavior of 3-D flows. The use of vorticity to analyze 3-D flows has been previously reported in the literature [44–47]. Particularly, Kolář et al. [44] introduced the vortex-identification Q-criterion and λ_2 to understand the high shear zones around an inclined flat plate, and this method presented good results in regions of strong shearing.

Both the Q-criterion and λ_2 criterion are used in computational fluid dynamics (CFD) and numerical simulations to visualize and analyze vortical structures in 3-D flows.

In general, it has been noted in the literature that barrier-type mixers and double entry of each segment into the mixer can both lead to improved mixing quality [22,48–50].

The advantages of using a T-micromixer with helical elements for microfluidic energy applications are multi-fold. The introduction of helical elements significantly enhances mixing performance compared to traditional T-mixers. The chaotic advection induced by the helical structures promotes rapid mixing, reducing the required mixing length and increasing reaction rates. Micromixers are characterized by low power requirements, and the utilization of helical elements allows for even more efficient mixing with reduced energy consumption. This aspect is particularly relevant for microfluidic energy applications, where energy efficiency is a critical consideration.

In the current work, the geometrical parameters are investigated further to enhance the mixing performance of the T-micro mixer for the application of microfluidics in the field of renewable energy. The mixing performance in T-microkenics and the interaction of flow behavior index with Reynolds number, the kinematic extents, and the geometrical factors were numerically examined using the validated CFD models. The results of the simulation were compared to those of the base-type micromixer in the literature. From these results, it may be concluded that the introduction of helical elements within the T-micromixer design offers a promising approach to enhancing microfluidic energy applications. The improved mixing efficiency makes it a compelling choice for various energy-related processes.

2. Methodology

2.1. Biogas Production and Characterization

In this work, biogas was generated as described in a previous study by our research group [51]. Briefly, vine shoots obtained from a local vineyard placed in Extremadura, Spain, during the vine trimming process served as the raw material for this study. Firstly, 10 g of vine shoots were heated at 800 °C in air (200 mL min^{-1}) for 8 min.

The gases produced during the gasification process of the vine shoots were analyzed with the aid of a KONIK-HRGC-400-A Gas Chromatograph equipped with a TCD detector and an automatic injection valve.

The composition of the exhaust biogas resulting from the gasification of vine shoots (in moles of biogas per kilogram of vine shoot) was as follows: H_2, 0.69; CO, 1.86; CO_2, 0.51; CH_4, 1.49; C_2H_2, 0.02; C_2H_4, 0.44; and C_2H_6, 0.08. The lower heating value (LHV), as determined following a method described elsewhere [52], resulted in 5.3 $MJ{\cdot}m^{-3}$ (STP).

2.2. Governing Equations and Numerical Methodology

The governing equations of incompressible steady flow have been achieved numerically using CFD code (ANSYS Fluent 2016, [53]). The mass conservation and momentum equations and the species and diffusion equations are expressed as follows:

$$div\vec{V} = 0 \tag{1}$$

$$\rho\vec{V}{\cdot}\nabla\vec{V} = -\nabla P + \mu\nabla^2\vec{V} \tag{2}$$

$$\vec{V}{\cdot}\nabla C = D\nabla^2 C \tag{3}$$

where V denotes the velocity, ρ is the fluid density, μ the viscosity, P is the static pressure, D is the diffusion coefficient, and C is the concentration.

The degree of mixing is computed as follows to determine the mixing efficiency of micromixers with various geometrical factors and flow conditions [54]:

$$M = 1 - \frac{\sigma}{\sigma_0} \tag{4}$$

where σ is the standard deviation of the mole fraction at a transverse cross-section defined as [55]:

$$\sigma^2 = \frac{1}{n}\sum_{i=1}^{n}(c_i - \bar{c})^2 \quad (5)$$

where n denotes the total number of samples, c_i : the mole concentration at a position on the cross-section measured, and $\bar{c}$ the average value of c_i. In the process of mixing, the two fluids are segregated at the beginning, and the standard deviation can be written as:

$$\sigma_0^2 = \bar{c}(1 - \bar{c}) \quad (6)$$

2.3. Deformation and Vorticity Intensity

The transport equation of the vorticity Ω is given by [44]:

$$\frac{\delta\vec{\Omega}}{\delta t} + \vec{V}\cdot\vec{\nabla}\vec{\Omega} = \vec{\Omega}\cdot\vec{\nabla}\vec{V} + v\Delta\vec{\Omega} \quad (7)$$

The deformation process achieves high-quality mixing by molecular diffusion, and the vorticity process realizes fine macroscopic homogenization. These parameters are given as follows:

$$D = \left[2\left(\frac{\partial u}{\partial x}\right)^2 + 2\left(\frac{\partial v}{\partial y}\right)^2 + 2\left(\frac{\partial w}{\partial z}\right)^2 + \left(\frac{\partial u}{\partial y} + \frac{\partial v}{\partial x}\right)^2 + \left(\frac{\partial u}{\partial z} + \frac{\partial w}{\partial x}\right)^2 + \left(\frac{\partial v}{\partial z} + \frac{\partial w}{\partial y}\right)^2\right]^{\frac{1}{2}} \quad (8)$$

$$\Omega = \frac{1}{2}\left[\left(\frac{\partial w}{\partial y} - \frac{\partial v}{\partial z}\right)^2 + \left(\frac{\partial u}{\partial z} - \frac{\partial w}{\partial x}\right)^2 + \left(\frac{\partial v}{\partial x} - \frac{\partial u}{\partial y}\right)^2\right]^{\frac{1}{2}} \quad (9)$$

Evolutions of the mean deformation (D_{mean}) and rotation rates (Ω_{mean}) in the T-shaped channel are presented in the following equations]:

$$D_{mean} = \frac{1}{\mho}\int S d\mho \quad (10)$$

$$\Omega_{mean} = \frac{1}{\mho}\int \Omega d\mho \quad (11)$$

where $\mho$ is the total volume of the fluid in the channel and S is the strain rate.

2.4. Velocity Gradient Tensor Method

The Q-criterion [44,45] defines vertices of (3-D) incompressible flow in the regions in which the magnitude vorticity reigns over the magnitude strain rate and translates as:

$$Q = \frac{1}{2}\left(\| \Omega \|^2 - \| S \|^2\right) > 0 \quad (12)$$

2.5. Geometries Description

The geometry of the simulated model (Figure 1) is inspired by the static mixerKenics (KM). The 3D geometry of the micromixers that were studied and built is considered in this study. A series of six repetitive pieces of micro-helical are assembled at a choice of connection angles and consist of the mixing elements embedded in the pipe. A T-shaped structure was used to permit the two fluids to be mixed. The assembled helical inserts have an overall length of 9 mm and an inner diameter of 1.5 mm. Each element has a thickness, t, equal to 0.05 mm and a length of 1.5 mm. The first and last helical elements are placed at a distance of 1.5 mm and 2.5 mm from the tube inlet and the tube outlet, respectively. The input sample is composed of Fluid A (the biogas described under Section 2.1) and Fluid

B (oxygen), 50% of each. The flow rate was $7 \cdot \times 10^{-4}$ kg/s, and the starting velocity was 0.01 m/s. A color scale indicating mass fraction has been included when necessary.

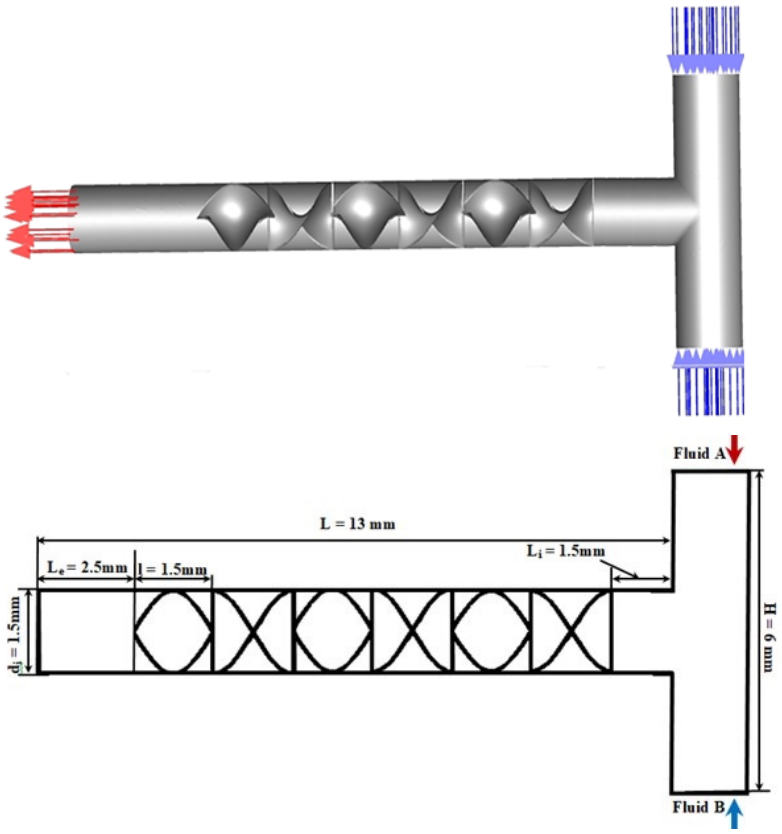

Figure 1. Schematic diagram of the T-microkenics.

The effect of blade twist (α) is examined, and four geometrical patterns are investigated for this purpose, which are: θ = 0°, 30°, 45°, 60°, and 90° (Figure 2).

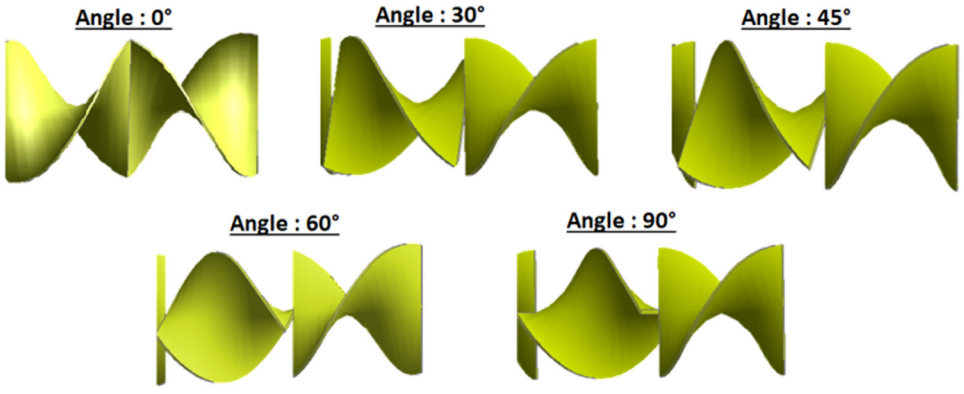

Figure 2. Schematic illustration of the helical element inserts with connection angles of 0°, 30°, 45°, 60°, and 90°.

2.6. Boundary Conditions

The boundary condition of the T-microchannel wall is a no-slip condition with zero flux of sample concentration and atmospheric pressure at the outlet, and all walls are considered adiabatic. Equal flow rates were considered at both inlets. These conditions have been widely used in studies focused on microchannels [56,57].

2.7. Grid Independency Test

A mesh independence test [58] was performed to determine the optimal cell size for the models and to ensure that the solution is independent of the mesh size.

Result variations are not important after the mesh size of 290,496 cells (Table 1); thus, this can be considered the improved mesh for the calculation. When compared to the finer mesh, this mesh size produces better results in less time.

Table 1. Grid-dependency test.

Mesh	Standard Deviation (SD)	ΔP (Pa)
80,916	0.01943	33.51
121,425	0.02136	33.87
192,947	0.02448	34.25
250,494	0.02647	34.42
290,496	0.02807	34.5
379,703	0.02815	34.65

2.8. CFD Code Validation

A quantitative evaluation has been realized for Newtonian fluids to ensure the numerical solutions obtained by the CFD code, the mixing performance, and the pressure drop were verified at various Reynolds numbers next to numerical simulations of mixing value in a microchannel T-junction from Kurnia et al. [59]. Figure 3 clearly shows how well our results match those from Kurnia et al.

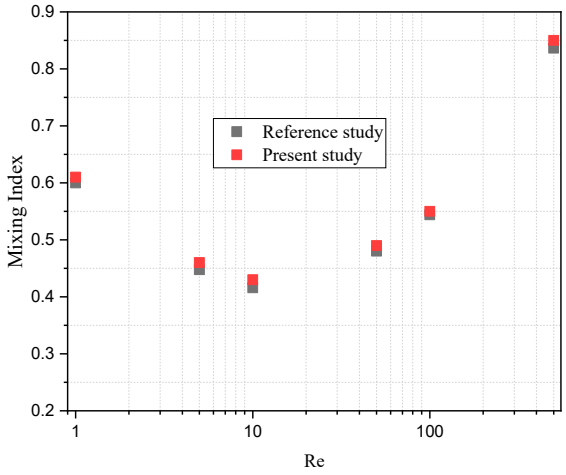

Figure 3. Comparison of current CFD results for mixing index for different Reynolds numbers with the results of Kurnia et al.

Validation can be displayed in terms of RMSE relative to the actual mixing index. To calculate RMSE (the root mean squared error), we calculate the residual (the difference between our numerical values and those of Kurnia et al.) and then take the square root of the average of the residuals.

The root mean square error can be expressed as:

$$RSME = \sqrt{\frac{1}{N}\sum_{i=1}^{N}(\hat{y}_i - y_i)^2} \text{ Then, } \quad RSME = 0.01135057$$

where:

N = Total number of values

$\hat{y}_i$: Value of MI (mixing index) as a function of Re calculated by our CFD.

y_i : Value of MI as a function of Re calculated by Kurnia.

3. Results and Discussion

3.1. Effect of the Geometrical Factors

Geometric design plays an imperative role in power consumption and all mixing characteristics. For four crossing angles that are 0°, 30°, 60°, and 90°, the radial velocity distribution is shown in the vertical direction at 6 mm from the entrance (2nd helical) with Re = 20 (Figure 4). The velocity profile swiftly develops into a parabolic profile, with the velocity components increasing continuously until they reach their maximum at the middle of the length element and then decreasing until they reach their minimum values at the junction of two neighboring elements. The identical velocity profile will then be replicated for all mixer elements. Higher values are observed with the augmentation in the twist angle from 0° to 90°. This latter suggests that an increase in twist angle results in a dominant secondary flow, which, in turn, leads to an elimination of circulation regions so that the fluid is allowed to circulate completely. This is in good agreement with some results previously reported in the literature [60–62].

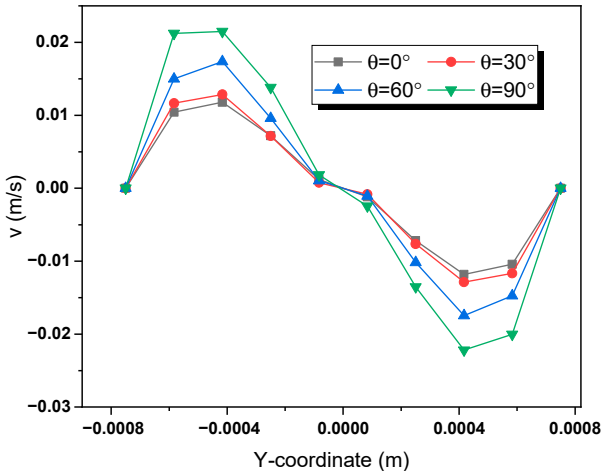

Figure 4. Velocities vs. mixer radius for various twisted angles at the 2nd helical and z = 0.006 m with Re = 20.

The variation in angles affects the geometry and leads to very different flow behavior. The changes in angle can create velocity gradients across the cross-section of the micromixer; these gradients result in variation in flow velocity, and increasing angles promote more complex flow patterns such as vortices, which can impact flow velocity. Also, a sharp angle may cause localized variations in velocity, leading to regions of higher and lower flow velocities.

In Figure 5, the effect of Reynolds numbers of the fluid on the vortex intensity within four cases of angles is presented. The secondary flow and the vorticity amplified quickly with the Reynolds number for all microkenics. Figure 5 clearly shows that, at low values of Re, scarce differences can be found in vortex intensities. On the contrary, differences become evident from Re = 20 and above. This fact evinces that an increase in the Reynolds number results in more intense secondary flows. Consequently, the fluid particles become more agitated, and the deformation of the fluid layers is favored [63].

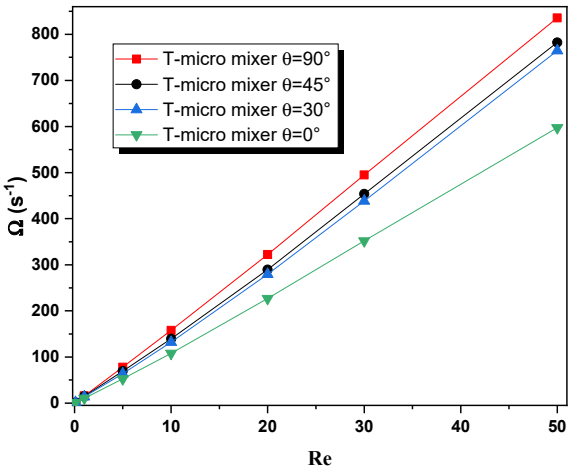

Figure 5. Evaluation of vortex intensity with various twisted angles for different Reynolds numbers.

Twisted angles also seem to play an important role in this case. The strength of the chaotic flows was compared at four twisted angles. Figure 5 also shows that, while the chaotic advection and the transversal movements of the particle fluid increased and the axial dispersion decreased, the vorticity process reached high-quality macroscopic homogenization. For twist angle θ = 90° the best fluid homogenization was achieved. It becomes evident that for 90° the flows were strong, leading to high kinematic energy. Consequently, the dynamic flow is a key parameter to increase the chaotic flow inside microkenics [64].

It was clear from Figure 6 that the deformation rate increases as the Reynolds number and twisted angle do. This indicates that the deformation process results in good mixing quality [65]. Despite the progressions being in low regimes, they were quite close to one another, thus the deformation rate had less impact on the secondary flow, and the flow easily went through the micromixers.

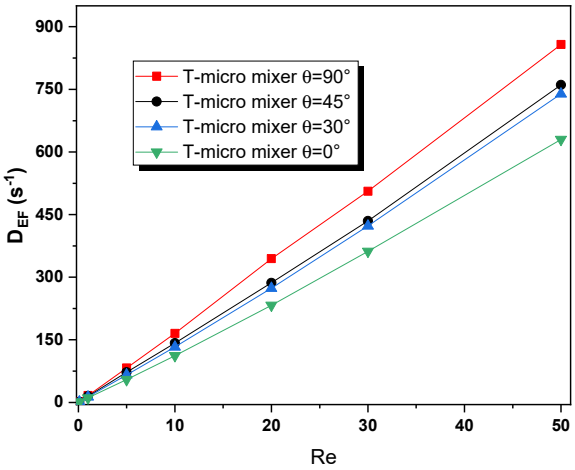

Figure 6. Evolution of deformation intensity with various twisted angles for different Reynolds numbers.

3.2. Application of the Vortex Identification Method

As indicated in Section 2, in this work, the Q-criterion has been used as the vortex identification method [66].

Figure 7 depicts the evolution of the Q*-criterion as a function of Reynolds number Re for different twisted angles (from 0° to 90°). From this figure, it can be clearly seen that this parameter increases constantly with the increase in the Reynolds number. While going towards the lowest values of θ, the vortex intensity grows to be important. While the θ

values are lower, the fluid is more viscous, and hence, more energy is required to create an important agitation in the fluid. At very low Reynolds number values, the chaotic behavior is not yet active, and molecular diffusion is dominant. Thus, these phenomena are identical, regardless of what the value of θ is.

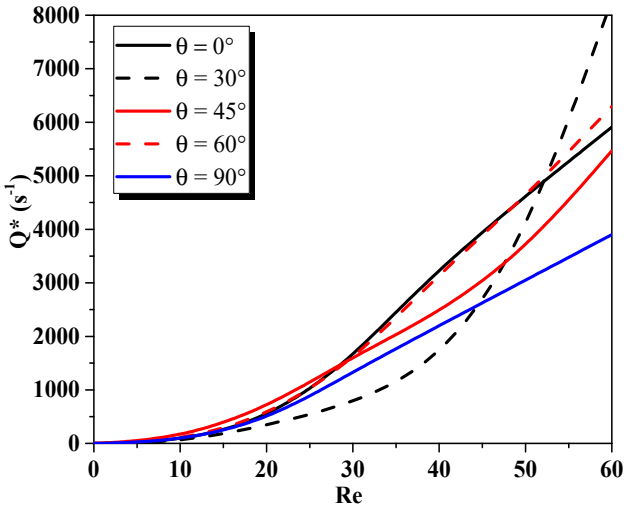

Figure 7. Evolutions of the Q*-criterion in the fluid flow for the Reynolds number in the Kenics micromixer with varying twisted angles.

3.3. Mixing Performance

The mixing performance in Figure 8 was calculated at the exit of the T-micromixer with a Reynolds number between 0.1 and 50 for the four twisted angles (0°, 30°, 45°, and 90°).

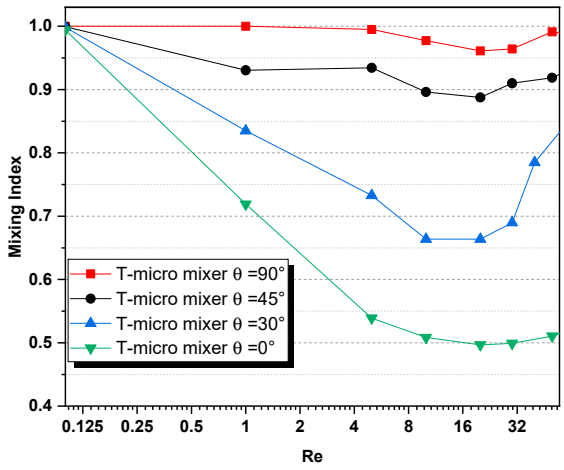

Figure 8. Development of mixing index with various twisted angles for different Reynolds numbers.

The observed difference between the results of different geometries is remarkable. Simulation demonstrated that the helicals with θ = 90° and θ = 45° show much higher mixing performance than those with θ = 0° and 30°. The geometry with θ = 90° has considerably higher mixing index values due to the highly chaotic advection impact compared to the other twisted angles of the T-micromixer.

As displayed in Figure 9a,b, the simulation showed that the T-kenics had the best rates of blending compared with the other micromixers, the planar micromixers [67] and a passive interdigital micromixer [68] due to the chaotic advection impact, which proves the high fluid homogenization. This is in line with other results previously reported [69,70]. In T-shaped micromixers, for low values of the Reynolds number, the mixing performance is usually low, mainly because segregation of the fluid streams may occur. However, at

higher values of the Reynolds number, symmetry decreases, and the so-called *engulfment flow regime* appears, which results in a sudden increase in the mixing performance [71]. In other words, under very low Re conditions (e.g., Re = 0.125), high mixing efficiencies are obtained, as depicted in Figure 9a. This behavior is attributable to the long residence time of fluids in the mixing channel under these particular conditions, which results in the occurrence of an almost exclusively diffusive mechanism. This, in turn, remarkably slows down the mixing process.

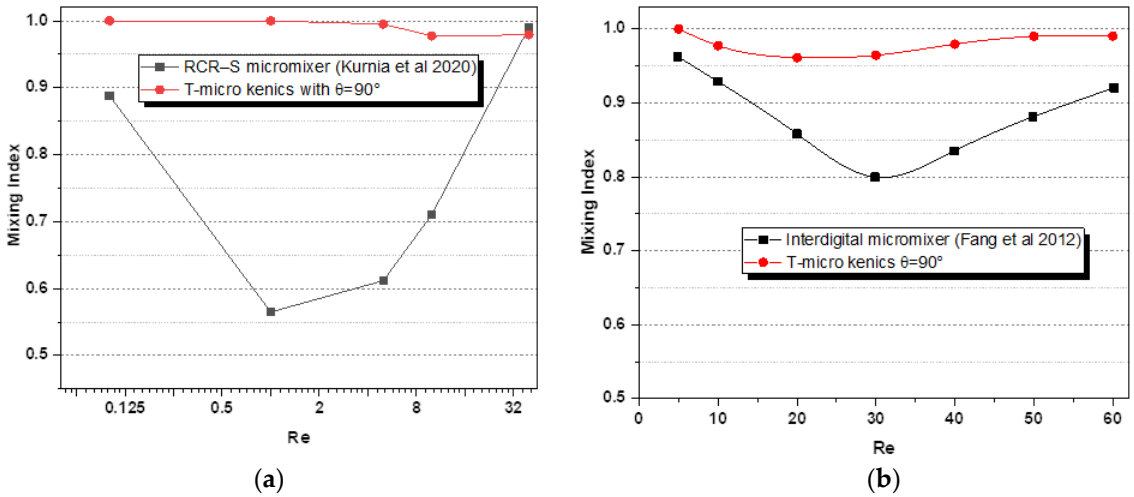

Figure 9. Evaluation of mixing efficiency vs. Reynolds numbers with RCR-S (**a**) and interdigital (**b**) micromixers [59,68].

On the contrary, as Re increases, advection progressively becomes the dominant transport condition. In this case, the effect of molecular diffusion is much less important. Thus, residence times continuously decrease, and mixing efficiency drops, reaching a minimum for Re = 30. Yet, at Re values equal to 40 and above, the engulfment flow regime is generated, and mixing performance increases, as can be seen in Figure 9b.

Figure 10 shows the evolution of the mixing index calculated along the Kenics micromixer from the first plane to the channel exit, precisely in transverse planes, for Re = 103. In comparison with other designs of T-micromixers with two different embedded microbarriers [72], we can see from this figure the advantage of the T-kenics, where the MI grows progressively and reaches high values approaching the exit plane in all cases.

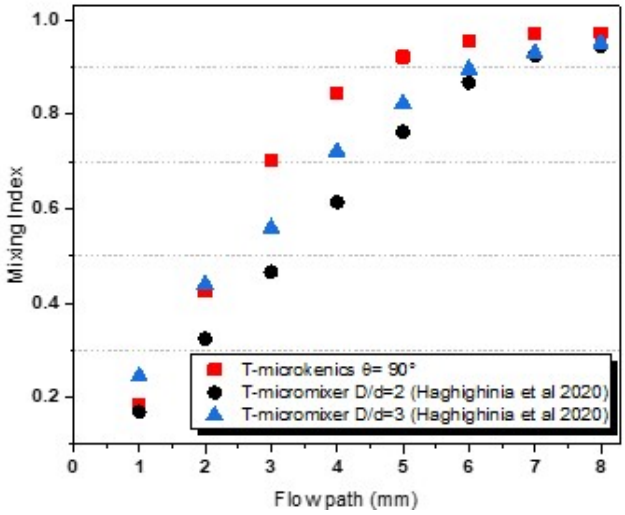

Figure 10. Evaluation of mixing efficiency vs. flow path with various micromixers [72].

As the micromixer has barriers and obstacles that can stretch and split the flow, even in laminar flows, these structures induce chaotic flow patterns, leading to enhanced mixing.

Figure 10 indicates that Mixing Indexes for the Kenics micro mixer reach values well above 0.9. Hence, it can be concluded that mixing performance can be increased through an alternative structural design of the micromixer. Particularly if vortex-inducing obstacles are introduced in the path of fluid flow, the advection process becomes progressively dominant over the diffusion one, with the subsequent improvement of the mixing performance [70,73].

3.4. Pressure Drop

The pressure drop is a significant characteristic of the flow. With microkenics ($\theta = 90°$), we evaluate the results of the expected geometry with the recent geometry from Cheri et al. [67] and Fan et al. [74] in a range of Reynolds numbers (0.2–50). We observed that the choice of microkenics had a lower possible pressure drop than the other two micromixers (Figure 11a,b).

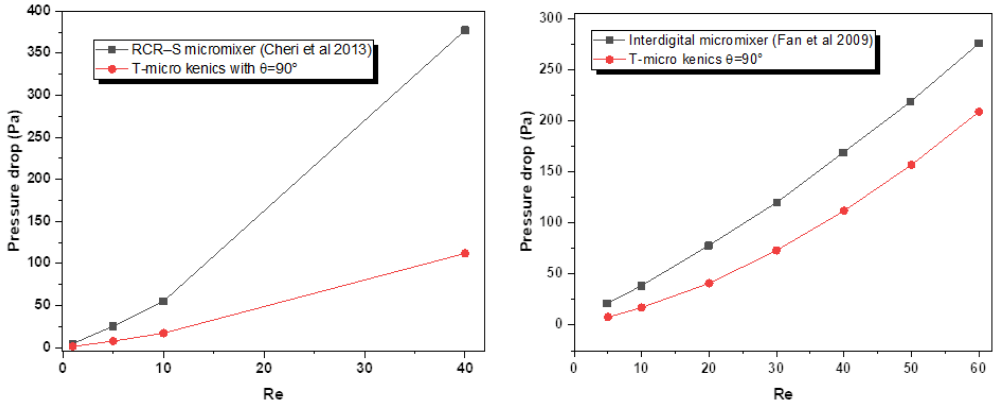

Figure 11. Pressure loss vs. Reynolds number for RCR-S (**a**) and interdigital (**b**) micromixers [67,74].

The effect of pressure drops in micromixers is closely related to the flow behavior and mixing performance within the microchannels. Pressure drop can significantly influence the flow regime in micromixers, and this, in turn, affects the mixing efficiency. Higher pressure drops can lead to faster flow rates, which can promote convective mixing but may also increase energy consumption. Hence, a less remarkable pressure drop, as is the case with the proposed micromixer, results in better flow behavior and mixing efficiency within microchannels.

Figure 12 indicates that the pressure loss increases when the twist angle is increased from 0° to 90°. In a micromixer, the relationship between pressure loss (or pressure drop) and Reynolds number can vary significantly depending on the design and orientation of the microchannel, particularly when considering different twisted angles. However, at low Reynolds numbers (typically, Re < 100), flows within microchannels are mostly laminar. In this regime, pressure loss is primarily influenced by the fluid viscosity and channel geometry rather than the twisted angle. For various twisted angles, one might expect relatively small differences in pressure loss at low Reynolds numbers. The impact of the twisted angle is likely to be minimal, and pressure loss will follow a typical laminar flow trend, increasing linearly with flow rate. This appears to be the case with the micromixer under study. From Figures 11 and 12, it can be concluded that, for low values of Re, pressure drop values are low. On the contrary, at higher values of Re, complex flow patterns are generated, and, as a consequence, the pressure difference between inlets and outlets increases remarkably. Usually, pressure drops reach their maximum value when the aforementioned engulfment flow regime appears. Hence, it may be stated that pressure drop and mixing efficiency follow a reverse trend [75,76].

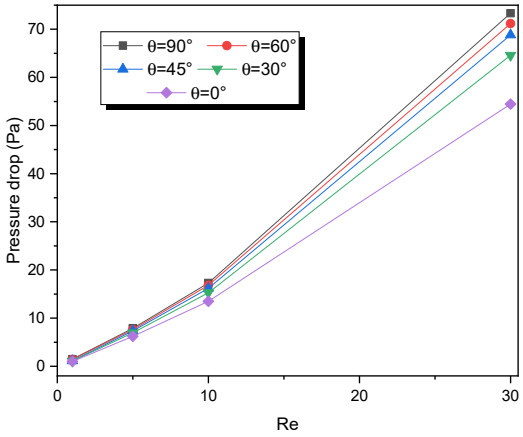

Figure 12. Pressure loss vs. Reynolds number for different twisted angles.

3.5. Contour of Mass Fraction

The mass fraction was computed repeatedly at spaced locations on the intersection plane between every two helical elements from the first element until the exit (plane 8) of the micromixer with $\theta = 90°$ and two values of Reynolds Re = 1 and 50 (Figure 13). The flow behavior presented by the mass fraction contours shows that the fluid layers for P1 to P4 advance in a different mode. On Re = 1, where molecular diffusion is predominant, the intensity of homogenization of the concentration layers was realized at a fourth plane much faster than the second at Re = 50, which was achieved at the fifth plane.

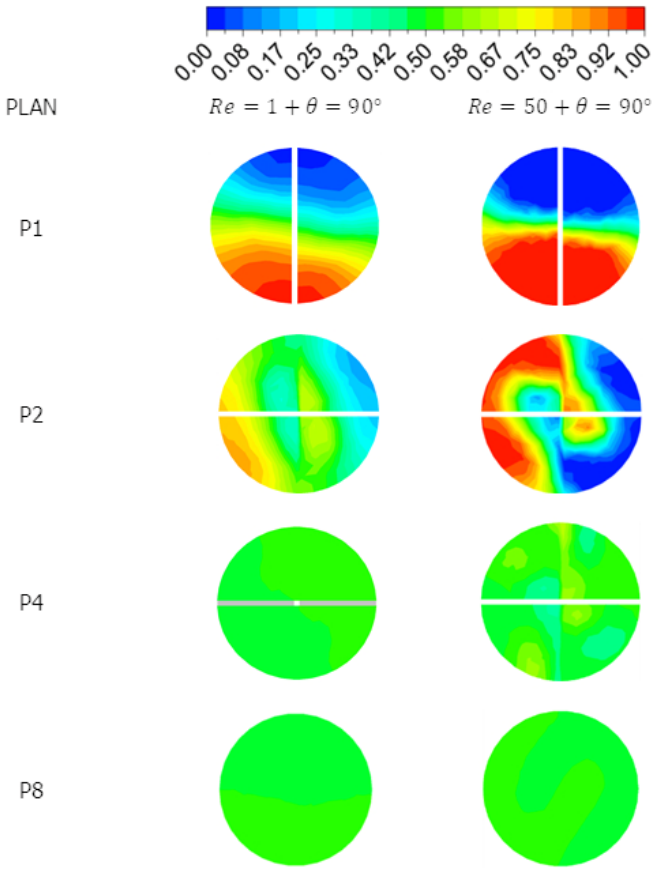

Figure 13. Cross-sectional profiles of mass fraction distribution calculated in kenics with connection angle $\theta = 90°$ and flow with Re = 1 and Re = 50.

The effects of the twisted angles of the helical and Reynolds numbers on the mechanism of the chaotic mixture were qualitatively analyzed by presenting the fracture profiles of the mass fraction in Figure 14a,b.

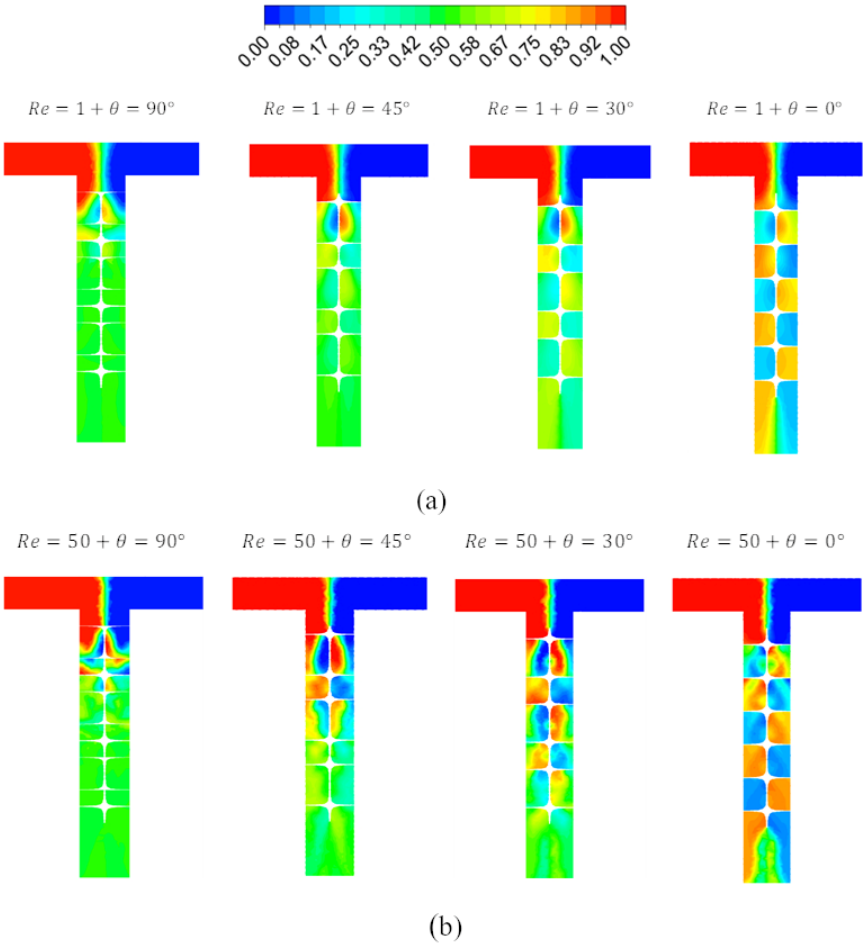

Figure 14. Mass fraction distribution for different twisted angles. (**a**) *Re* = 1; (**b**) *Re* = 50.

The mass fraction distribution in a micromixer can vary significantly for different twisted angles, particularly at different Reynolds numbers (Re). At Re = 1, the flow is in the laminar regime. In this regime, the influence of the twisted angle on the mass fraction distribution may be relatively limited. The primary mechanism driving mixing is molecular diffusion. Different twisted angles may induce varying degrees of secondary flows and vortices within the microchannel. These secondary flows can enhance mixing by increasing the interaction between fluid layers and promoting radial mixing.

Contrarily, at Re = 50, the flow is in the transitional regime, which means it exhibits characteristics of both laminar and turbulent flow. In this regime, the effect of the twisted angle on the mass fraction distribution can become more significant. The twisted geometry can induce vortices and secondary flows, which can help accelerate mixing. Consequently, different twisted angles can result in varying degrees of turbulence and secondary flow patterns. A more pronounced twisted angle might generate more intense vortices and improve mixing efficiency. Hence, more significant variations in the mass fraction distribution for different twisted angles compared to the laminar regime can be observed.

In summary, the effect of twisted angles on mass fraction distribution in a micromixer depends on the Reynolds number. At Re = 1, the impact of the twisted angle is relatively limited due to the dominance of diffusion-driven mixing. At Re = 50, the twisted angle can significantly influence the mass fraction distribution by enhancing mixing through secondary flows and vortices. The specific details of how the mass fraction distribution

varies for different twisted angles would require experimental or computational analysis of the particular micromixer geometry and operating conditions. The fluid gradually splits into several thinner layers as the flow continues. Thus, the interface area is enlarged quickly with Re = 1, which is interpreted by the phenomenon of molecular diffusion, and the maximum performance of the mixture, whatever the value of the Reynolds number, is improved in the T-mixer with $\theta = 90^{\circ}$. The homogeneous mixture indicates the efficiency of these T-kenics.

4. Conclusions

The mixing performance of a T-micromixer with helical elements inserted at different angles has been numerically studied in the flow field of Reynolds numbers ranging from 0.1 to 60 by using a CFD approach. The micromixer is composed of six helical elements, and the flow stream was changed every 1.5 mm for the reason that the elements were connected at chosen twisted angles of 0°, 30°, 45°, 60°, and 90° to split, recombine, and rearrange the flow component. Vortex intensity has been investigated by a new method based on the idea that vorticity overtakes deformation in the vortex.

The T-micro kenics can potentially achieve an exceedingly high mixing produced within a short mixing length in microchannels. It was found by the micro-vortex identification method, kinematics behavior, and mixing efficiency that the geometric with helical elements twisted at an angle of 90° inserted in the T-micromixer significantly increases the mixing performance. The performance of mixing and the pressure losses in this micromixer with a chosen angle were evaluated and compared with the topical numerical data, and the numerical results show a much higher quality of mixing with fewer pressure losses.

This underscores the potential of microfluidic approaches, exemplified by the T-micromixer, to significantly improve the energy production from biogas obtained from renewable sources like vine shoot waste, thereby advancing bioenergy generation in alignment with sustainable development goals.

These findings open up several exciting future prospects in the fields of microfluidics and bioenergy generation. Future research could delve deeper into optimizing the angles of helical elements within micromixers. Exploring angles beyond the ones studied, or even using variable angles within a single micromixer, may further enhance mixing performance. Scaling up the T-micromixer design and evaluating its performance at a bench or semiindustrial scale could be an important avenue. Understanding how this technology performs in larger setups can facilitate its practical application in biogas production on an industrial level. Finally, within a holistic approach, the simultaneous optimization of multiple parameters, including micromixer geometry, fluid properties, and operating conditions, still remains an attractive challenge.

Author Contributions: A.M.: Investigation, Visualization, Writing—Original Draft; N.T.T.: Investigation, Formal analysis, Writing—Original Draft; K.R.: Conceptualization, Data curation, Writing—Original Draft; A.A.-K.: Conceptualization, Data curation, Writing—Original Draft; E.M.C.-C.: Conceptualization, Methodology, Writing—Original Draft, Supervision. All authors have read and agreed to the published version of the manuscript.

Funding: This research received no external funding.

Data Availability Statement: Data will be made available on request.

Conflicts of Interest: The authors declare no conflict of interest.

References

1. Kan, X.; Zhou, D.; Yang, W.; Zhai, X.; Wang, C.-H. An Investigation on Utilization of Biogas and Syngas Produced from Biomass Waste in Premixed Spark Ignition Engine. *Appl. Energy* **2018**, *212*, 210–222. [CrossRef]
2. Ramos, A.; Monteiro, E.; Rouboa, A. Biomass Pre-Treatment Techniques for the Production of Biofuels Using Thermal Conversion Methods—A Review. *Energy Convers. Manag.* **2022**, *270*, 116271. [CrossRef]
3. Fan, F.; Wang, S.; Yang, S.; Hu, J.; Wang, H. Numerical Investigation of Gas Thermal Property in the Gasification Process of a Spouted Bed Gasifier. *Appl. Therm. Eng.* **2020**, *181*, 115917. [CrossRef]

4. Dabiri, S.; Kumar, P.; Rauch, W. Integrating Biokinetics with Computational Fluid Dynamics for Energy Performance Analysis in Anaerobic Digestion. *Bioresour. Technol.* **2023**, *373*, 128728. [CrossRef] [PubMed]
5. Li, Y.; Yang, S.; Feng, F.; Tagawa, K. A Review on Numerical Simulation Based on CFD Technology of Aerodynamic Characteristics of Straight-Bladed Vertical Axis Wind Turbines. *Energy Rep.* **2023**, *9*, 4360–4379. [CrossRef]
6. Aly, A.M.; Clarke, J. Wind Design of Solar Panels for Resilient and Green Communities: CFD with Machine Learning. *Sustain. Cities Soc.* **2023**, *94*, 104529. [CrossRef]
7. Khan, Z.U.; Ali, Z.; Uddin, E. Performance Enhancement of Vertical Axis Hydrokinetic Turbine Using Novel Blade Profile. *Renew. Energy* **2022**, *188*, 801–818. [CrossRef]
8. Shiehnejadhesar, A.; Schulze, K.; Scharler, R.; Obernberger, I. A New Innovative CFD-Based Optimisation Method for Biomass Combustion Plants. *Biomass Bioenergy* **2013**, *53*, 48–53. [CrossRef]
9. Gao, H.; Runstedtler, A.; Majeski, A.; Boisvert, P.; Campbell, D. Optimizing a Woodchip and Coal Co-Firing Retrofit for a Power Utility Boiler Using CFD. *Biomass Bioenergy* **2016**, *88*, 35–42. [CrossRef]
10. Jahangiri, A.; Ebrahim Sarbandi Farahani, M.; Ahmadi, G.; Shahsavar, A.; Borzouei, A.; Gharehbaei, H. Coupled CFD and 3E (Energy, Exergy and Economical) Analysis of Using Windbreak Walls in Heller Type Cooling Towers. *J. Clean. Prod.* **2022**, *358*, 131550. [CrossRef]
11. Zheng, L.; Lu, W.; Wu, L.; Zhou, Q. A Review of Integration between BIM and CFD for Building Outdoor Environment Simulation. *Build. Environ.* **2023**, *228*, 109862. [CrossRef]
12. Santiago, J.L.; Borge, R.; Martin, F.; de la Paz, D.; Martilli, A.; Lumbreras, J.; Sanchez, B. Evaluation of a CFD-Based Approach to Estimate Pollutant Distribution within a Real Urban Canopy by Means of Passive Samplers. *Sci. Total Environ.* **2017**, *576*, 46–58. [CrossRef] [PubMed]
13. Wen, T.; Lu, L.; He, W.; Min, Y. Fundamentals and Applications of CFD Technology on Analyzing Falling Film Heat and Mass Exchangers: A Comprehensive Review. *Appl. Energy* **2020**, *261*, 114473. [CrossRef]
14. Satjaritanun, P.; Khunatorn, Y.; Vorayos, N.; Shimpalee, S.; Bringley, E. Numerical Analysis of the Mixing Characteristic for Napier Grass in the Continuous Stirring Tank Reactor for Biogas Production. *Biomass Bioenergy* **2016**, *86*, 53–64. [CrossRef]
15. Birth, T.; Heineken, W.; He, L. Preliminary Design of a Small-Scale System for Theconversion of Biogas to Electricity by HT-PEM Fuel Cell. *Biomass Bioenergy* **2014**, *65*, 20–27. [CrossRef]
16. Santana, H.S.; Tortola, D.S.; Silva, J.L.; Taranto, O.P. Biodiesel Synthesis in Micromixer with Static Elements. *Energy Convers. Manag.* **2017**, *141*, 28–39. [CrossRef]
17. Banerjee, R.; Kumar, S.P.J.; Mehendale, N.; Sevda, S.; Garlapati, V.K. Intervention of Microfluidics in Biofuel and Bioenergy Sectors: Technological Considerations and Future Prospects. *Renew. Sustain. Energy Rev.* **2019**, *101*, 548–558. [CrossRef]
18. Šalić, A.; Zelić, B. A Game Changer: Microfluidic Technology for Enhancing Biohydrogen Production—Small Size for Great Performance. *Energies* **2022**, *15*, 7065. [CrossRef]
19. Alam, A.; Kim, K.-Y. Analysis of Mixing in a Curved Microchannel with Rectangular Grooves. *Chem. Eng. J.* **2012**, *181–182*, 708–716. [CrossRef]
20. Chen, J.; Risberg, M.; Westerlund, L.; Jansson, U.; Lu, X.; Wang, C.; Ji, X. A High Efficient Heat Exchanger with Twisted Geometries for Biogas Process with Manure Slurry. *Appl. Energy* **2020**, *279*, 115871. [CrossRef]
21. Stroock, A.D.; Dertinger, S.K.; Whitesides, G.M.; Ajdari, A. Patterning Flows Using Grooved Surfaces. *Anal Chem.* **2002**, *74*, 5306–5312. [CrossRef]
22. Tseng, L.-Y.; Yang, A.-S.; Lee, C.-Y.; Hsieh, C.-Y. CFD-Based Optimization of a Diamond-Obstacles Inserted Micromixer with Boundary Protrusions. *Eng. Appl. Comput. Fluid Mech.* **2011**, *5*, 210–222. [CrossRef]
23. Liu, R.H.; Stremler, M.A.; Sharp, K.V.; Olsen, M.G.; Santiago, J.G.; Adrian, R.J.; Aref, H.; Beebe, D.J. Passive Mixing in a Three-Dimensional Serpentine Microchannel. *J. Microelectromech. Syst.* **2000**, *9*, 190–197. [CrossRef]
24. Kim, D.; Shin, J.; Son, Y.; Park, S. Characteristics of In-Cylinder Flow and Mixture Formation in a High-Pressure Spray-Guided Gasoline Direct-Injection Optically Accessible Engine Using PIV Measurements and CFD. *Energy Convers. Manag.* **2021**, *248*, 114819. [CrossRef]
25. Kim, D.S.; Lee, S.H.; Kwon, T.H.; Ahn, C.H. A Serpentine Laminating Micromixer Combining Splitting/Recombination and Advection. *Lab Chip* **2005**, *5*, 739–747. [CrossRef] [PubMed]
26. Valera-Medina, A.; Vigueras-Zuniga, M.O.; Baej, H.; Syred, N.; Chong, C.T.; Bowen, P.J. Outlet Geometrical Impacts on Blowoff Effects When Using Various Syngas Mixtures in Swirling Flows. *Appl. Energy* **2017**, *207*, 195–207. [CrossRef]
27. Ottino, J.M. *The Kinematics of Mixing: Stretching, Chaos, and Transport*; Cambridge University Press: Cambridge, UK, 1989; ISBN 9780521368780.
28. Tian, F.; Zhang, M.; Fan, H.; Gu, M.; Wang, L.; Qi, Y. Numerical Study on Microscopic Mixing Characteristics in Fluidized Beds via DEM. *Fuel Process. Technol.* **2007**, *88*, 187–198. [CrossRef]
29. Karvelas, E.; Liosis, C.; Karakasidis, T.; Sarris, I. Mixing of Particles in Micromixers under Different Angles and Velocities of the Incoming Water. *Proceedings* **2018**, *2*, 577. [CrossRef]
30. Mahmud, F.; Tamrin, K.F.; Mohamaddan, S.; Watanabe, N. Effect of Thermal Energy and Ultrasonication on Mixing Efficiency in Passive Micromixers. *Processes* **2021**, *9*, 891. [CrossRef]
31. Bothe, D.; Lojewski, A.; Warnecke, H.-J. Computational Analysis of an Instantaneous Chemical Reaction in a T-Microreactor. *AIChE J.* **2010**, *56*, 1406–1415. [CrossRef]

32. Lobasov, A.S.; Minakov, A.V.; Kuznetsov, V.V.; Rudyak, V.Y.; Shebeleva, A.A. Investigation of Mixing Efficiency and Pressure Drop in T-Shaped Micromixers. *Chem. Eng. Process. Process Intensif.* **2018**, *134*, 105–114. [CrossRef]
33. Wong, S.H.; Ward, M.C.L.; Wharton, C.W. Micro T-Mixer as a Rapid Mixing Micromixer. *Sens. Actuators B Chem.* **2004**, *100*, 359–379. [CrossRef]
34. Stroock, A.D.; Dertinger, S.K.W.; Ajdari, A.; Mezić, I.; Stone, H.A.; Whitesides, G.M. Chaotic Mixer for Microchannels. *Science* **2002**, *295*, 647–651. [CrossRef] [PubMed]
35. Silva, J.P.; dos Santos, A.; Semiao, V. Experimental Characterization of Pulsed Newtonian Fluid Flows inside T-Shaped Micromixers with Variable Inlets Widths. *Exp. Therm. Fluid Sci.* **2017**, *89*, 249–258. [CrossRef]
36. Chen, J.; Hai, Z.; Lu, X.; Wang, C.; Ji, X. Heat-Transfer Enhancement for Corn Straw Slurry from Biogas Plants by Twisted Hexagonal Tubes. *Appl. Energy* **2020**, *262*, 114554. [CrossRef]
37. Hoffmann, M.; Schlüter, M.; Räbiger, N. Experimental Investigation of Liquid–Liquid Mixing in T-Shaped Micro-Mixers Using μ-LIF and μ-PIV. *Chem. Eng. Sci.* **2006**, *61*, 2968–2976. [CrossRef]
38. Maionchi, D.D.O.; Ainstein, L.; dos Santos, F.P.; de Souza Júnior, M.B. Computational Fluid Dynamics and Machine Learning as Tools for Optimization of Micromixers Geometry. *Int. J. Heat Mass Transf.* **2022**, *194*, 123110. [CrossRef]
39. Zhu, S.; Fang, Y.; Chen, Y.; Yu, P.; Han, Y.; Xiang, N.; Ni, Z. Stackable Micromixer with Modular Design for Efficient Mixing over Wide Reynold Numbers. *Int. J. Heat Mass Transf.* **2022**, *183*, 122129. [CrossRef]
40. Cortes-Quiroz, C.A.; Azarbadegan, A.; Zangeneh, M. Evaluation of Flow Characteristics That Give Higher Mixing Performance in the 3-D T-Mixer versus the Typical T-Mixer. *Sens. Actuators B Chem.* **2014**, *202*, 1209–1219. [CrossRef]
41. Gobby, D.; Angeli, P.; Gavriilidis, A. Mixing Chacteristics of T-Type Microfluidic Mixers. *J. Micromech. Microeng.* **2001**, *11*, 126–132. [CrossRef]
42. Kim, D.S.; Lee, S.W.; Kwon, T.H.; Lee, S.S. A Barrier Embedded Chaotic Micromixer. *J. Micromech. Microeng.* **2004**, *14*, 798–805. [CrossRef]
43. Bertsch, A.; Heimgartner, S.; Cousseau, P.; Renaud, P. Static Micromixers Based on Large-Scale Industrial Mixer Geometry. *Lab Chip* **2001**, *1*, 56–60. [CrossRef] [PubMed]
44. Kolář, V.; Šístek, J.; Cirak, F.; Moses, P. Average Corotation of Line Segments near a Point and Vortex Identification. *AIAA J.* **2013**, *51*, 2678–2694. [CrossRef]
45. Cucitore, R.; Quadrio, M.; Baron, A. On the Effectiveness and Limitations of Local Criteria for the Identification of a Vortex. *Eur. J. Mech. B Fluids* **1999**, *18*, 261–282. [CrossRef]
46. Jeong, J.; Hussain, F. On the Identification of a Vortex. *J. Fluid Mech.* **1995**, *285*, 69–94. [CrossRef]
47. Lappa, M.; Inam, S. Large Eddy Simulation of Three-Dimensional Hybrid Forced-Buoyancy Convection in Channels with a Step. *Int. J. Heat Mass Transf.* **2023**, *202*, 123767. [CrossRef]
48. Chen, L.; Wang, G.; Lim, C.; Seong, G.H.; Choo, J.; Lee, E.K.; Kang, S.H.; Song, J.M. Evaluation of Passive Mixing Behaviors in a Pillar Obstruction Poly(Dimethylsiloxane) Microfluidic Mixer Using Fluorescence Microscopy. *Microfluid. Nanofluid.* **2009**, *7*, 267–273. [CrossRef]
49. Santana, H.S.; Silva, J.L.; Tortola, D.S.; Taranto, O.P. Transesterification of Sunflower Oil in Microchannels with Circular Obstructions. *Chin. J. Chem. Eng.* **2018**, *26*, 852–863. [CrossRef]
50. Soleymani, A.; Kolehmainen, E.; Turunen, I. Numerical and Experimental Investigations of Liquid Mixing in T-Type Micromixers. *Chem. Eng. J.* **2008**, *135*, S219–S228. [CrossRef]
51. Gañán, J.; Al-Kassir Abdulla, A.; Cuerda Correa, E.M.; Macías-García, A. Energetic Exploitation of Vine Shoot by Gasification Processes. A Preliminary Study. *Fuel Process. Technol.* **2006**, *87*, 891–897. [CrossRef]
52. Gañan, J.; González, J.F.; González-García, C.M.; Cuerda-Correa, E.M.; Macías-García, A. Determination of the Energy Potential of Gases Produced in the Pyrolysis Processes of the Vegetal Carbon Manufacture Industry. *Bioresour. Technol.* **2006**, *97*, 711–720. [CrossRef] [PubMed]
53. Mebarki, B.; Mohammed, K.; Imtiaz, M.; Belkacem, D.; Medal, M.; Benhanifia, K.; Jamshed, W.; Eid, M.R.; El Din, S.M. A CFD Examination of Free Convective Flow of a Non-Newtonian Viscoplastic Fluid Using ANSYS Fluent. *Arab. J. Chem.* **2023**, *16*, 105309. [CrossRef]
54. Boss, J. Evaluation of the Homogeneity Degree of a Mixture. *Bulk Solids Handl.* **1986**, *6*, 1207–1215.
55. Ishii, K.; Hihara, E.; Munakata, T. Mechanism of Temperature-Difference-Induced Spiral Flow in Microchannel and Investigation of Mixing Performance of a Non-Invasive Micromixer. *Appl. Therm. Eng.* **2020**, *174*, 115291. [CrossRef]
56. Sohankar, A.; Riahi, M.; Shirani, E. Numerical Investigation of Heat Transfer and Pressure Drop in a Rotating U-Shaped Hydrophobic Microchannel with Slip Flow and Temperature Jump Boundary Conditions. *Appl. Therm. Eng.* **2017**, *117*, 308–321. [CrossRef]
57. Hajmohammadi, M.R.; Alipour, P.; Parsa, H. Microfluidic Effects on the Heat Transfer Enhancement and Optimal Design of Microchannels Heat Sinks. *Int. J. Heat Mass Transf.* **2018**, *126*, 808–815. [CrossRef]
58. Ding, H.; Xie, P.; Ingham, D.; Ma, L.; Pourkashanian, M. Flow Behaviour of Drop and Jet Modes of a Laminar Falling Film on Horizontal Tubes. *Int. J. Heat Mass Transf.* **2018**, *124*, 929–942. [CrossRef]
59. Kurnia, J.C.; Sasmito, A.P. Performance Evaluation of Liquid Mixing in a T-Junction Passive Micromixer with a Twisted Tape Insert. *Ind. Eng. Chem. Res.* **2020**, *59*, 3904–3915. [CrossRef]

60. Zimparov, V. Prediction of Friction Factors and Heat Transfer Coefficients for Turbulent Flow in Corrugated Tubes Combined with Twisted Tape Inserts. Part 1: Friction Factors. *Int. J. Heat Mass Transf.* **2004**, *47*, 589–599. [CrossRef]
61. Fazel, Z.; Sadrhosseini, H.; Hannani, S.K. Heat Transfer Intensification of Turbulent Forced Convection by Inserting Discontinuous Twisted Tapes in a Wavy Tube; Hydrothermal and Thermodynamics Analysis. *Chem. Eng. Process. Process Intensif.* **2022**, *181*, 109137. [CrossRef]
62. Singh, I.; Vardhan, S. Experimental Investigation of an Evacuated Tube Collector Solar Air Heater with Helical Inserts. *Renew. Energy* **2021**, *163*, 1963–1972. [CrossRef]
63. Douroum, E.; Kouadri, A.; Tahiri, A.; Brihmat, M.; Khelladi, S. Hydrodynamic and Kinematic Study to Analyze the Mixing Efficiency of Short Passive Micromixers. *Ind. Eng. Chem. Res.* **2022**, *61*, 5994–6009. [CrossRef]
64. Wang, X.; Liu, Z.; Wang, B.; Cai, Y.; Wan, Y. Vortices Degradation and Periodical Variation in Spiral Micromixers with Various Spiral Structures. *Int. J. Heat Mass Transf.* **2022**, *183*, 122168. [CrossRef]
65. Naas, T.T.; Hossain, S.; Aslam, M.; Rahman, A.; Hoque, A.S.M.; Kim, K.-Y.; Riazul Islam, S.M. Kinematic Measurements of Novel Chaotic Micromixers to Enhance Mixing Performances at Low Reynolds Numbers: Comparative Study. *Micromachines* **2021**, *12*, 364. [CrossRef] [PubMed]
66. Hinge, S.P.; Patwardhan, A.W. Thermal-Hydraulic Performance of an Annular Pipe with Square Wire Coil Inserts Using Computational Fluid Dynamics. *Ind. Eng. Chem. Res.* **2020**, *59*, 3887–3903. [CrossRef]
67. Sadegh Cheri, M.; Latifi, H.; Salehi Moghaddam, M.; Shahraki, H. Simulation and Experimental Investigation of Planar Micromixers with Short-Mixing-Length. *Chem. Eng. J.* **2013**, *234*, 247–255. [CrossRef]
68. Fang, Y.; Ye, Y.; Shen, R.; Zhu, P.; Guo, R.; Hu, Y.; Wu, L. Mixing Enhancement by Simple Periodic Geometric Features in Microchannels. *Chem. Eng. J.* **2012**, *187*, 306–310. [CrossRef]
69. Tan, S.J.; Yu, K.H.; Ismail, M.A.; Teoh, Y.H. Enhanced Liquid Mixing in T-Mixer Having Staggered Fins. *Asia Pac. J. Chem. Eng.* **2020**, *15*, e2538. [CrossRef]
70. Wu, C.-Y.; Lai, B.-H. Numerical Study of T-Shaped Micromixers with Vortex-Inducing Obstacles in the Inlet Channels. *Micromachines* **2020**, *11*, 1122. [CrossRef]
71. Mariotti, A.; Galletti, C.; Brunazzi, E.; Salvetti, M.V. Mixing Sensitivity to the Inclination of the Lateral Walls in a T-Mixer. *Chem. Eng. Process. Process Intensif.* **2022**, *170*, 108699. [CrossRef]
72. Haghighinia, A.; Movahedirad, S.; Rezaei, A.K.; Mostoufi, N. On-Chip Mixing of Liquids with High-Performance Embedded Barrier Structure. *Int. J. Heat Mass Transf.* **2020**, *158*, 119967. [CrossRef]
73. Irfan, M.; Shah, I.; Niazi, U.M.; Ali, M.; Ali, S.; Jalalah, M.S.; Asif Khan, M.K.; Almawgani, A.H.M.; Rahman, S. Numerical Analysis of Non-Aligned Inputs M-Type Micromixers with Different Shaped Obstacles for Biomedical Applications. *Proc. Inst. Mech. Eng. Part E J. Process Mech. Eng.* **2022**, *236*, 870–880. [CrossRef]
74. Fan, Y.; Hassan, I. The Numerical Simulation of a Passive Interdigital Micromixer with Uneven Lamellar Width. In Proceedings of the 7th International Conference on Nanochannels, Microchannels, and Minichannels, Pohang, Republic of Korea, 22–24 June 2009; pp. 813–819.
75. Okuducu, M.B.; Aral, M.M. Novel 3-D T-Shaped Passive Micromixer Design with Helicoidal Flows. *Processes* **2019**, *7*, 637. [CrossRef]
76. Silva, A.O.; Monteiro, C.A.A.; Souza, V.P.D.; Ferreira, A.S.; Jaimes, R.P.; Fontoura, D.V.R.; Nunhez, J.R. Fluid Dynamics and Reaction Assessment of Diesel Oil Hydrotreating Reactors via CFD. *Fuel Process. Technol.* **2017**, *166*, 17–29. [CrossRef]

Disclaimer/Publisher's Note: The statements, opinions and data contained in all publications are solely those of the individual author(s) and contributor(s) and not of MDPI and/or the editor(s). MDPI and/or the editor(s) disclaim responsibility for any injury to people or property resulting from any ideas, methods, instructions or products referred to in the content.